Mapping Earth's Gravitation Using GRACE Data

Pavel Novák, Gerrit Austen, Mohammad A. Sharifi, and Erik W. Grafarend

Stuttgart University, Department of Geodesy and Geoinformatics,
Geschwister-Scholl-Strasse 24/D, 70174 Stuttgart, Germany
pnovak@gis.uni-stuttgart.de

Summary. This article describes an approach for global mapping of the Earth's gravitational field developed, tested and successfully implemented at the Geodetic Institute of the Stuttgart University. The method is based on the Newtonian equation of motion that relates satellite-to-satellite tracking (SST) data observed by the two satellites of the Gravity Recovery And Climate Experiment (GRACE) directly to unknown spherical harmonic coefficients of the Earth's gravitational potential (geopotential). Observed values include SST data observed both in the low-low (inter-satellite range, velocity and acceleration) and the high-low (satellites' positions) mode. The low-low SST data specific for the time being to the GRACE mission are available through a very sensitive K-band ranging system. The high-low SST data are then provided by on-board Global Positioning System (GPS) receivers. The article describes how the mathematical model can be modified. The geopotential is approximated by a truncated series of spherical harmonic functions. An alternative approach based on integral inversion of the GRACE data into the geopotential is also formulated and discussed. The article also presents sample numerical results obtained by testing the model using both simulated and observed data. Simulation studies suggest that the model has a potential for recovery of the Stokes coefficients up to degree and order 120. Intermediate results from the analysis of actual data have a lower resolution.

Key words: GRACE mission, geopotential, satellite-to-satellite tracking, Stokes's coefficients, Green's integrals

1 Introduction

Current satellite missions dedicated to the global mapping of the Earth's gravitational field provide data that can be inverted into global models of the gravitational potential (geopotential). The US-German satellite mission Gravity Recovery And Climate Experiment (GRACE) launched on March 17, 2002 is based on two spacecraft following each other along almost circular (approximate eccentricity of 0.001), low (decaying altitude during the lifetime of

the mission from 500 to 300 km) and polar orbits (approximate inclination of 89°). The satellites fly approximately 220 ± 50 km apart. During the expected five-year lifetime of the mission, the relative motion of the two satellites is measured using a very sensitive K-band ranging system that senses changes in separation between the two satellites. Moreover, the GRACE satellites are equipped with geodetic-quality Global Positioning System (GPS) receivers allowing for accurate orbit determination as well as accelerometers measuring non-gravitational forces affecting the satellites. The mission is thus based on satellite-to-satellite tracking (SST) in both the low-low (LL) and high-low (HL) mode. More information on the mission can be found for example in (Tapley and Reigber, 1998).

This article discusses the inversion of the GRACE SST data into the geopotential and its parameters. The method is based on their direct relationship through the Newtonian equation of motion (Reubelt et al., 2003). Three modifications of this equation are proposed: (i) balancing the vector of the inter-satellite acceleration differences with corresponding differences of the geopotential gradients, both projected into the inter-satellite direction, and representing the geopotential in a form of a finite spherical harmonics series expansion (e.g. Rummel et al. , 1978; Austen and Grafarend, 2005); (ii) Approach (i) modified by expanding the gradient of the geopotential at the barycentre of the two GRACE satellites, i.e., dealing with the GRACE satellites as a large one-directional gradiometer (Keller and Hess, 1998); (iii) replacing the gradient difference of the geopotential by a boundary integral of the Abel-Poisson type and solving the geopotential at a reference surface of known geometry. While the first two approaches aim at recovery of spectral description of the geopotential (Stokes's coefficients), the last approach allows for description of the geopotential on a known boundary surface outside Earth's masses.

2 SST data of type GRACE

In this section, the GRACE observables are shortly reviewed. Starting with the HL-SST, positions of the GRACE satellites in the terrestrial (Earth-fixed) geocentric coordinate system can be derived from GPS code and carrier beat phase observations. Corresponding position vectors are defined in terms of the geocentric terrestrial Cartesian coordinates (vectors and matrices are bold)

$$\mathbf{x} = [\, x \quad y \quad z \,]^T \,. \tag{1}$$

Note that the argument of time related to all values in (1) was omitted. The space segment of the GRACE mission consists of the two satellites following each other along a similar orbit. Let us assign the leading satellite with the index 1 and the trailing satellite with the index 2. Positions of the satellites and their derivatives will be then labeled with corresponding indices. Besides the

position of the satellites, also their velocity vector as well as the acceleration vector

$$\dot{\mathbf{x}} \;=\; [\; \dot{x} \quad \dot{y} \quad \dot{z} \;]^T \;, \qquad \ddot{\mathbf{x}} \;=\; [\; \ddot{x} \quad \ddot{y} \quad \ddot{z} \;]^T \;, \tag{2}$$

are being used in the following derivations. An operator δ for differences between parameters corresponding to the positions of the two satellites is used throughout the article. Vector differences in position, velocity and acceleration are then given as follows:

$$\delta\mathbf{x} \;=\; \mathbf{x}_2 \;-\; \mathbf{x}_1 \;, \qquad \delta\dot{\mathbf{x}} \;=\; \dot{\mathbf{x}}_2 \;-\; \dot{\mathbf{x}}_1 \;, \qquad \delta\ddot{\mathbf{x}} \;=\; \ddot{\mathbf{x}}_2 \;-\; \ddot{\mathbf{x}}_1 \;. \tag{3}$$

The LL-SST provides the inter-satellite range, e.g. (Blaha, 1992),

$$\varrho \;=\; \sqrt{<\delta\mathbf{x} \mid \delta\mathbf{x}>} \;=\; \mid \delta\mathbf{x} \mid \;. \tag{4}$$

Considering the unit vector of the inter-satellite direction

$$\mathbf{e} \;=\; [\; e_x \quad e_y \quad e_z \;]^T \;=\; \frac{\delta\mathbf{x}}{\varrho} \;, \tag{5}$$

the LL-SST data can be used for derivation of the first-order time derivative of the range called herein inter-satellite velocity e.g. (Blaha, 1992)

$$\dot{\varrho} \;=\; <\delta\dot{\mathbf{x}} \mid \mathbf{e}> \;+\; <\delta\mathbf{x} \mid \dot{\mathbf{e}}> \;=\; <\delta\dot{\mathbf{x}} \mid \mathbf{e}> \;, \tag{6}$$

since

$$<\delta\mathbf{x} \mid \dot{\mathbf{e}}> \;=\; 0 \;. \tag{7}$$

Finally, the LL-SST also provides the second-order time derivative of the range called inter-satellite acceleration, e.g. (Rummel, 1980),

$$\ddot{\varrho} \;=\; <\delta\ddot{\mathbf{x}} \mid \mathbf{e}> \;+\; <\delta\dot{\mathbf{x}} \mid \dot{\mathbf{e}}> \;=\; <\delta\ddot{\mathbf{x}} \mid \mathbf{e}> \;+\; \frac{\mid \delta\dot{\mathbf{x}} \mid^2 \;-\; \dot{\varrho}^2}{\varrho} \;. \tag{8}$$

The second term on the right-hand side of (8) is sometimes referred to as a *velocity correction*. The velocity correction accounts for the fact that the GRACE assembly with its inter-satellite direction $\mathbf{e}$ forms a moving observational system in inertial space.

3 Mathematical model

In the inertial reference frame, acceleration of a unit-mass satellite can be expressed according to Newton's law of motion as follows

$$\ddot{\mathbf{X}} \;=\; -\,\nabla V(\mathbf{X}) \;+\; \mathbf{A} \;, \tag{9}$$

where the standard sign convention is used. The vector $\mathbf{A}$ stands for the non-gravitational acceleration vector and completes formally the model. No other gravitating masses are considered in (9) but the Earth's system. No tidal effects were considered during simulations but they completed the model in case of the real data analysis. Vectors in the inertial frame, that is usually approximated by the celestial frame, are denoted by capital letters. The transformation between the two coordinate systems can be done by the well known rotation matrix operator for transformation between the terrestrial and celestial frames (McCarthy and Petit, 2004). The matrix rotating the celestial to terrestrial coordinate system is denoted as $\mathbf{M}$. At the epoch t of the observation

$$\mathbf{x}(t) \;=\; \mathbf{M}(t)\;\mathbf{X}(t)\;. \tag{10}$$

It is assumed that the geopotential V in (9) represents the gravitational potential of the rotating Earth, i.e., various direct and indirect tidal effects as well as loading effects can successfully be modelled. This concerns namely the real data analysis. We can write the inter-satellite acceleration vector of the GRACE satellites in the inertial (celestial) reference system as follows:

$$\delta\ddot{\mathbf{X}} \;=\; -\,\delta\nabla V(\mathbf{X}) \;+\; \delta\mathbf{A}\;, \tag{11}$$

with the inter-satellite non-gravitational acceleration vector $\delta\mathbf{A}$.

Combining (8) and (9), the observation equation for the first approach of type *acceleration differences* can be written in the form

$$\frac{\mid \delta\dot{\mathbf{x}} \mid^2 \;-\; \dot{\varrho}^2}{\varrho} \;-\; \ddot{\varrho} \;=< \delta\nabla V(\mathbf{x}) \mid \mathbf{e} >\;, \tag{12}$$

where the geopotential gradient vectors correspond to the terrestrial geocentric Cartesian coordinate system. The velocity difference $\mid \delta\dot{\mathbf{x}} \mid$, which has to be derived by numerically differentiation from kinematic HL-SST positions, is the critical quantity for the quality of the geopotential solution in any of the proposed models. For its evaluation, see e.g. (Austen and Grafarend, 2005). Note that the non-gravitational acceleration vector difference $\delta\mathbf{A}$ is omitted starting with (12). This component was included neither in the simulated nor real data analysis.

Expanding the gradient of the geopotential at the barycenter of the two GRACE satellites leads to the second approach. Since the GRACE satellites are at any time of a similar mass, the position vector of their barycentre B can approximately be estimated as follows:

$$\mathbf{x}_B \;\doteq\; \frac{\mathbf{x}_1 \;+\; \mathbf{x}_2}{2}\;. \tag{13}$$

The geopotential gradient at the position of the first satellite can be related to the barycentre

$$\nabla_1 V(\mathbf{x}) \doteq \nabla_B V(\mathbf{x}) + \nabla_B \otimes \nabla_B V(\mathbf{x}) \ (\mathbf{x}_1 - \mathbf{x}_B) \ . \tag{14}$$

The linear term of the expansion was only considered in (14). Similarly

$$\nabla_2 V(\mathbf{x}) \doteq \nabla_B V(\mathbf{x}) + \nabla_B \otimes \nabla_B V(\mathbf{x}) \ (\mathbf{x}_2 - \mathbf{x}_B) \ . \tag{15}$$

Keeping the linear approximation in mind, subtracting (14) from (15) yields

$$\delta\nabla V(\mathbf{x}) \doteq \nabla_B \otimes \nabla_B V(\mathbf{x}) \ \delta\mathbf{x} \ . \tag{16}$$

Substituting (16) into (12) results in the *linear gradiometry equation*

$$\frac{|\ \delta\dot{\mathbf{x}}\ |^2 - \dot{\varrho}^2}{\varrho^2} - \frac{\ddot{\varrho}}{\varrho} \doteq < \nabla_B \otimes \nabla_B V(\mathbf{x}) \ \mathbf{e} \mid \mathbf{e} > \ . \tag{17}$$

The linearization error represents the greatest problem for its applicability (Keller and Sharifi, 2005). On the other hand, the contribution of low-degree harmonics is the most dominant one. Therefore, the smaller the low-degree coefficients, the more accurate the linear model approximates.

In this regards, we consider one of the available geopotential models and utilize the low-degree coefficients of the model as a priori information. The right-hand side of (17), for instance, can be written as

$$< \nabla_B \otimes \nabla_B V(\mathbf{x}) \ \mathbf{e} \mid \mathbf{e} >$$

$$= < \nabla_B \otimes \nabla_B V_l(\mathbf{x}) \ \mathbf{e} \mid \mathbf{e} > \ + < \nabla_B \otimes \nabla_B V^l(\mathbf{x}) \ \mathbf{e} \mid \mathbf{e} > \ , \tag{18}$$

where V_l and V^l stand for the spheroidal reference field and the corresponding incremental one, respectively. Accordingly, the first term on the right-hand side of (18) is split into the approximate term and the respective correction

$$< \nabla_B \otimes \nabla_B V_l(\mathbf{x}) \ \mathbf{e} \mid \mathbf{e} >$$

$$= \underbrace{< \nabla_B \otimes \nabla_B V_{0l}(\mathbf{x}) \ \mathbf{e} \mid \mathbf{e} >}_{\text{approximate value}} + \underbrace{< \nabla_B \otimes \nabla_B \Delta V_l(\mathbf{x}) \ \mathbf{e} \mid \mathbf{e} >}_{\text{correction}} \ . \tag{19}$$

In order to reduce the linearization error, we retain the correction term and replace the approximate one with an equation similar to (12). Consequently, (17) can be recast into

$$\frac{|\ \delta\dot{\mathbf{x}}\ |^2 - \dot{\varrho}^2}{\varrho^2} - \frac{\ddot{\varrho}}{\varrho} - \frac{1}{\varrho} < \delta\nabla V_{0l}(\mathbf{x}) \mid \mathbf{e} >$$

$$\doteq < \nabla_B \otimes \nabla_B \left[\ \Delta V_l(\mathbf{x}) + V^l(\mathbf{x}) \ \right] \ \mathbf{e} \mid \mathbf{e} > \ . \tag{20}$$

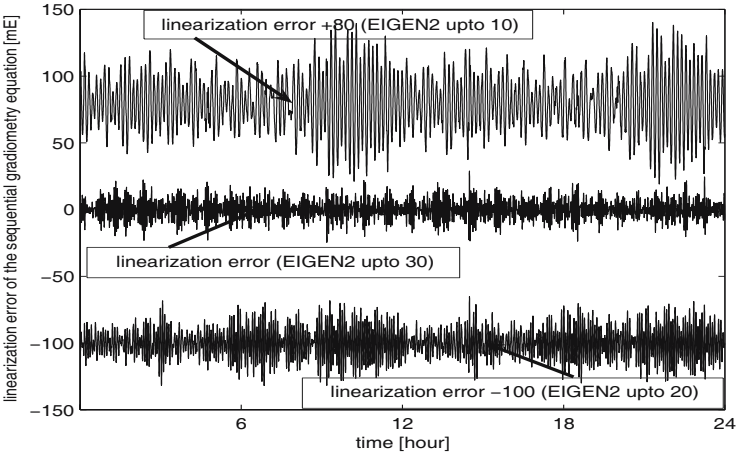

Fig. 1. Linearization error for the reference field of degree 10, 20 and 30

Equation (20) is known as the *sequential gradiometric observation equation*. It reduces the linearization error, differences between the left- and the right-hand sides of (20), dramatically. Figure 1 shows the linearization error for the reference field of degree 10, 20 and 30. The linearization error corresponding to the reference field of degree 30 is less than the observation random error (Keller and Sharifi, 2005). Note that the magnitude of the linearization errors for the full field may reach values at the level of 0.5 E.

Being one-point function and having a direct relation with the field geometry (curvature of the field at the point) are two noteworthy achievements of the alternative formulation. Besides, using an observation quantity, which is related to the second instead of the first order derivatives of the geopotential amplifies the high-frequency part of the signal. Since the transition from the first to the second order derivatives includes the application of a timely finite-differences scheme, the high-frequency part of the noise amplifies as well. Nevertheless, due to the different spectral behavior of signal and noise, in the end the second order approach leads to an improved resolution.

3.1 Spectral description of the geopotential

The geopotential satisfies everywhere outside the gravitating masses the Laplace differential equation

$$\nabla^2 V(\mathbf{x}) \;=\; 0\;, \tag{21}$$

where ∇^2 stands for the Laplacian. Thus the geopotential can be solved for in a form of a harmonic series. Not all coordinate systems are suitable for deriving

this solution, but knowing that the Earth and its equipotential surfaces are geometrically close to the sphere, geocentric spherical coordinates can be used

$$[\ r \quad \theta \quad \lambda\ ]^T = \left[\sqrt{x^2+y^2+z^2} \quad \arctan \frac{\sqrt{x^2+y^2}}{z} \quad \arctan \frac{y}{x} \right]^T , \quad (22)$$

with the geocentric radius r $(0 \leq r < \infty)$, reduced co-latitude θ $(0 \leq \theta \leq \pi)$ and longitude λ $(0 \leq \lambda < 2\pi)$, respectively. The solution of (21) can be then written for $r \geq R$

$$V(r,\theta,\lambda) \ = \ \sum_{n,m} \left(\frac{R}{r} \right)^{n+1} \ Y_{n,m}(\theta,\lambda)\ V_{n,m} \ , \quad (23)$$

with radius of the reference sphere R. The spherical harmonics $Y_{n,m}$ and the Stokes coefficients $V_{n,m}$ are both degree (n) and order (m) dependent (Abramowitz and Stegun, 1972). Substituting (23) (12), (17) and (20), respectively, results in systems of linear equations with vector-valued and tensor-valued spherical harmonics, respectively. In both cases, however, their projection to the inter-satellite direction $\mathbf{e}$ is considered. Unknown values then represent the Stokes coefficients.

3.2 Boundary-value description of the geopotential

According to (21), the geopotential is a harmonic function everywhere outside the Earth's system. This property is due to the Poisson differential equation that relates the gravitational potential and the mass density distribution of the gravitating masses. The geopotential is also regular at infinity, namely

$$V(\mathbf{x}) \ = \ \mathcal{O}\left(\ |\mathbf{x}|^{-1} \ \right) \ , \quad (24)$$

with the Landau symbol $\mathcal{O}$ describing in this particular case the attenuation of the geopotential with an increasing distance from the gravitating masses. Using an apparatus of Green's integrals, the solution of the Dirichlet boundary-value problem for the Laplace equation represents the well-known Abel-Poisson integral. It allows for evaluation of the geopotential at a general point P described by the geocentric radius vector $\mathbf{x}_P$ that is external to a boundary (simple smooth closed surface) on which the geopotential is known. The boundary must completely contain the gravitating masses. For the boundary S described by the geocentric radius vectors $\mathbf{y}$, this solution takes the form of the surface integral (Kellogg, 1929)

$$V(\mathbf{x}_P) \ = \ \frac{1}{S} \int_S \ V(\mathbf{y})\ \mathcal{K}(\mathbf{x}_P,\mathbf{y})\ dS(\mathbf{y}) \ . \quad (25)$$

In geodesy, one particular geocentric geometry is being used: the reference ellipsoid. Due to its symmetricity, the integral function $\mathcal{K}$ can be constructed.

Note that not all gravitating masses are imbedded inside the surface S. The gravitational potential of all external topographic and atmospheric masses is then either neglected or corrected for by an appropriate reduction. However, this is considered to be out of the scope of this article. Applying in (25) the gradient operator in the point P yields, cf. (Ardalan and Grafarend, 2004),

$$\nabla_P \, V(\mathbf{x}) \;=\; \frac{1}{S} \int_S V(\mathbf{y}) \; \nabla_P \, \mathcal{K}(\mathbf{x},\mathbf{y}) \; dS(\mathbf{y}) \;, \tag{26}$$

with vector-valued kernel function $\nabla\mathcal{K}$. Applying the matrix direct product on the gradient operator in the point P yields (van Gelderen and Rummel, 2001) and (Martinec, 2003),

$$\nabla_P \otimes \nabla_P \, V(\mathbf{x}) \;=\; \frac{1}{S} \int_S V(\mathbf{y}) \; \nabla_P \otimes \nabla_P \, \mathcal{K}(\mathbf{x},\mathbf{y}) \; dS(\mathbf{y}) \;, \tag{27}$$

with the tensor-valued kernel function $\nabla \otimes \nabla\mathcal{K}$.

Combining Eqs.(12) and (25) then results in the observation equation

$$\frac{|\, \delta\dot{\mathbf{x}} \,|^2 \;-\; \dot{\varrho}^2}{\varrho} \;-\; \ddot{\varrho} \;=\; \frac{1}{S} \int_S V(\mathbf{y}) \; \mathcal{H}(\mathbf{x}_1,\mathbf{x}_2,\mathbf{y}) \; dS(\mathbf{y}) \;, \tag{28}$$

with the scalar three-point kernel function

$$\mathcal{H}(\mathbf{x}_1,\mathbf{x}_2,\mathbf{y}) \;= < \delta\nabla\mathcal{K}(\mathbf{x},\mathbf{y}) \mid \mathbf{e} > \;. \tag{29}$$

For a single epoch, the integral kernel $\mathcal{H}$ relates the scalar geopotential at the reference ellipsoid to the functional on the left-hand side of (28) derived from the GRACE SST data that is a function of positions of the GRACE satellites. This makes the kernel function $\mathcal{H}$ different from typical integral kernels used in geodesy that usually relate two points only such as the Stokes, Hotine or Vening-Meinesz functions. Combining Eqs.(17) and (27) then results yet in another observation equation

$$\frac{|\, \delta\dot{\mathbf{x}} \,|^2 \;-\; \dot{\varrho}^2}{\varrho^2} \;-\; \frac{\ddot{\varrho}}{\varrho} \;=\; \frac{1}{S} \int_S V(\mathbf{y}) \; \mathcal{G}(\mathbf{x}_B,\mathbf{y}) \; dS(\mathbf{y}) \;, \tag{30}$$

with the scalar-valued integral kernel

$$\mathcal{G}(\mathbf{x}_B,\mathbf{y}) \;= < \nabla_B \otimes \nabla_B \; \mathcal{K}(\mathbf{x},\mathbf{y}) \; \mathbf{e} \mid \mathbf{e} > \;. \tag{31}$$

In this case, only the barycentre of the GRACE satellites and the computation point are related.

4 Numerical analysis

The models for recovery of the Stokes coefficients were extensively tested using both simulated and actual GRACE SST data. In this section, numerical tests of the model in (12) are described including the input data. The solution in a form of the boundary integrals is still to be investigated in details, namely its application for global gravity field studies.

4.1 Description of the synthetic GRACE data

The parameters on the left-hand side of Eqs.(12) and (17) are derived by combining the GRACE SST data. To verify the applicability of the model and to test the propagation of various observation errors, a series of numerical tests was performed. In-house generated synthetic data based on the EGM96 of degree and order 120, 160 and 200 were analyzed. The IAG Section II, SC7 one-month sample data based on the EGM96 of degree and order 300 and compiled by the Universities Bonn and Delft (IAG SC7, 2001) were also used. These test datasets provide noise-free inertial position, velocity and acceleration vectors of the GRACE satellites with a 5 second sampling interval. Noise-free simulated LL-SST observations were derived from these quantities. Finally, these noise-free SST data were also contaminated with correlated errors to study an effect of various errors on the accuracy of the solution.

Unfortunately, an actual level of correlation between HL-SST data of the two low-orbiting GRACE satellites is unknown. The same applies to two adjacent positions of a single satellite. Error simulation functions for GPS data, that correlate adjacent measurements through a Gauss-Markov process, were used in our study. This approach successfully applied by (Grafarend and Vaníček, 1980) for the weight estimation in levelling is based on recursive formulas that allow for simulation of the correlated observation noise. The level of correlation is controlled by a unitless correlation factor $0 \leq \beta \leq 1$, see (Austen and Grafarend, 2005) for details. Generally, $\beta = 0$ corresponds to uncorrelated errors and $\beta = 1$ to fully-correlated errors. In order to determine the accuracy of satellites' velocity vectors computed from noisy GPS positions by numerical differentiation, various empirical tests were performed. Noise-free simulated position data contaminated with errors of a varying magnitude and correlation behaviour were numerically differentiated to obtain the velocity vectors. They were afterwards compared to the noise-free simulated velocity vectors. Based on results of these tests, we concluded that the velocity of the GRACE satellites can be determined from their GPS positions with the accuracy better than 0.3 mm s^{-1}. Correlations between kinematic orbits of the two GRACE satellites were simulated by applying the same method with an offset to the GPS positions of the satellites. Such a coloured noise was added to noise-free simulated GPS positions in order to investigate the influence of the correlated GPS data on the geopotential solution.

4.2 Propagation of observation noise

In order to assess the ability of the proposed methods for the geopotential recovery, the influence of observation noise on the coefficients' estimation process was investigated. In this contribution, namely results based on the model in (12) are presented. Figure 2 illustrates how errors in the satellites' positions determined by GPS (here a 1 cm average error was assumed for each

coordinate) affect the geopotential solution. One can conclude that the overall quality of the solution strongly depends on the correlation of the position errors of both satellites. However, the analysis of synthetic data, described in this section, suggests that the Stokes coefficients up to degree and order 100 could be considered recoverable. Note that we define the maximum resolution of the model by the intersection of the signal and noise curves.

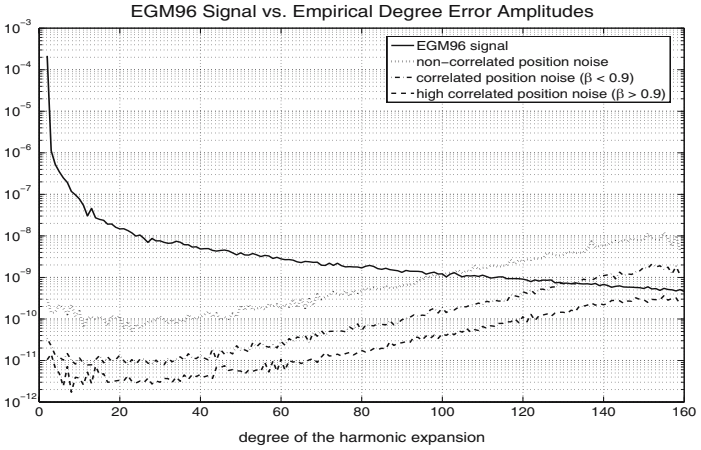

Fig. 2. Propagation of position errors ($\sigma_{x_i} = 1$ cm)

Figure 3 shows how the simulated noise in the velocity vectors of the two GRACE satellites influences the resolution of the computed model. The noise level of 0.1 mm/s is assumed for each component of the velocity vector. This noise arises from the fact that the velocity information has to be numerically derived from the noisy position vectors. As already mentioned before, noisy velocity information is the limiting factor of the overall solution quality. In absence of correlations between the two satellites' velocity vectors, i.e., for white noise, the geopotential recovery is limited to degree and order 70 given a noise level of 0.1 mm/s. To obtain the geopotential solution up to degree and order 100, the velocity errors of the GRACE satellites have to be correlated.

The impact of K-band measurement errors is displayed in Fig. 4. It can be concluded that relatively to other errors the inter-satellite position (1 cm) and inter-satellite velocity (1 μm/s) errors, that were used in our simulations, have no significant impact on the solution. Thus the GPS-based range can be used instead of the biased range from the K-band ranging system. In contrary, the effect of the inter-satellite acceleration errors is quite important. Figure 4 suggests that the accuracy of the inter-satellite acceleration at the level of 10^{-8} m/s^2 (1 μGal) is required to get the solution up to degree and order 100.

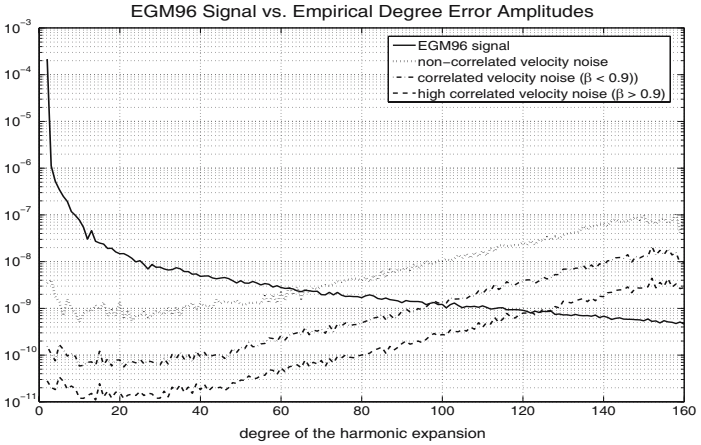

Fig. 3. Propagation of velocity errors ($\sigma_{\dot{x}_i} = 0.1$ mm/s)

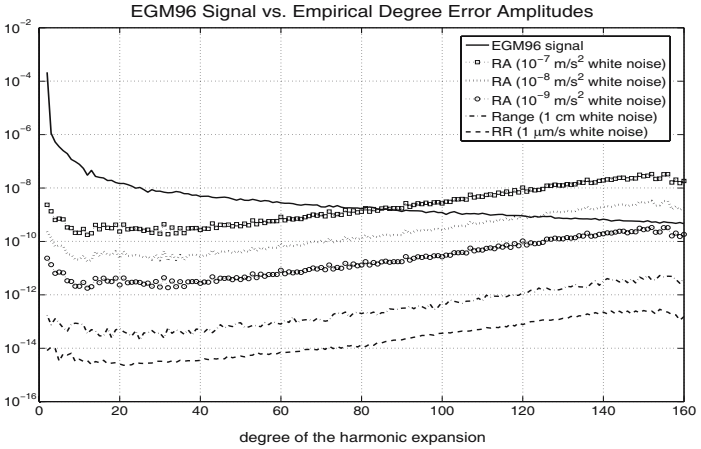

Fig. 4. Propagation of K-band measurement errors

Finally, the combined effect of all error influences (HL-SST: GPS and LL-SST: K-band) is presented in Fig. 5 for a pessimistic and optimistic mission scenario. Based on these results, the resolution of the recovered geopotential using the GRACE data and following the proposed method is expected to be in the range of degree and order 100 to 120.

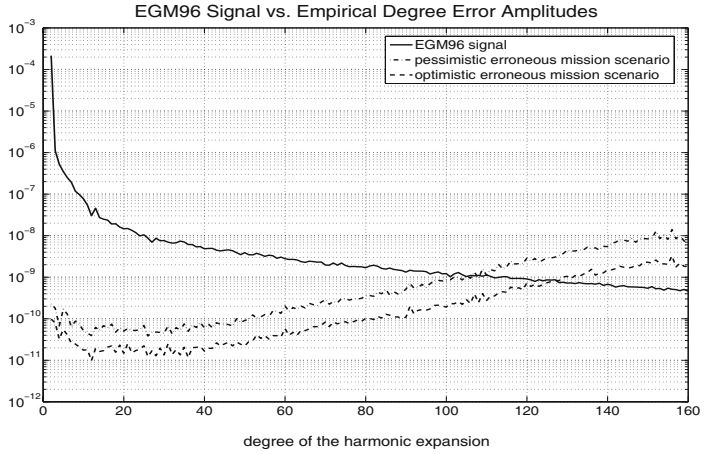

Fig. 5. Propagation of the combined measurement error influence

4.3 Processing actual GRACE data

The real data analysis was performed using approximately 88,000 observation values. The HL-SST data were kindly provided by Mr. Dražen Švehla of the Technical University Munich. Corresponding LL-SST data were then downloaded from the GRACE Data Center at the GeoForschungsZentrum (GFZ) Potsdam, Germany. Results presented in this article were extracted from 31 days of observations (03.230-03.260). Due to different sampling intervals of the data, the 30-second data were used.

Both the HL- and LL-SST data were routinely checked for outliers first. The HL-SST data were then rotated to the celestial frame and inter-satellite velocity differences were derived using numerical differentiation (Savitzky-Golay formula using the Fourier transform). This step is crucial for the approach and much attention was focused on its proper evaluation. To document the applicability of numerical differentiation schemes, Figure 6 shows an example of a comparison of intersatellite acceleration obtained by the numerical algorithm ($\varrho \rightarrow \ddot{\varrho}$) and those $\ddot{\varrho}$ provided by the GFZ Potsdam. Next, the observation vector is derived as a time series by the combination of HL- and LL-SST data according to the left-hand side of (12), see Fig. 7.

Further, the model was completed for tide-generated acceleration and reduced for a normal gravity field model. Finally, the Stokes coefficients up to degree and order 70 were recovered. The least-squares adjustment includes the computation of a full variance-covariance matrix, residuals as well as estimated a posteriori variance factor. Figure 8 shows the root mean square power spectrum of the recovered field as well as of its differences from the EIGEN-GRACE2S model of the GFZ Potsdam. Color Fig. XXIII on p. 299 then represents the synthesized differences between the recovered model and

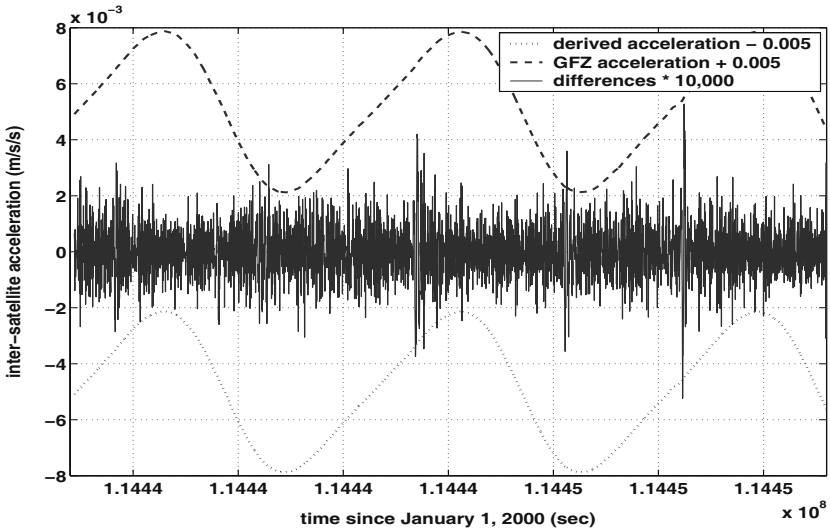

Fig. 6. Verifying the differentiation procedure using GRACE LL-SST data

the EIGEN-GRACE2S model. The maximum difference is 4.94 m and the global root mean square fit is 27 cm.

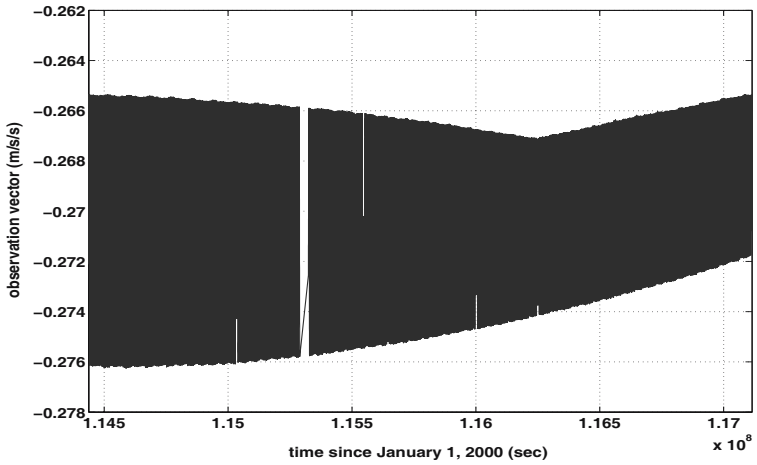

Fig. 7. Left-hand side of (12) based on actual GRACE HL- and LL-SST data

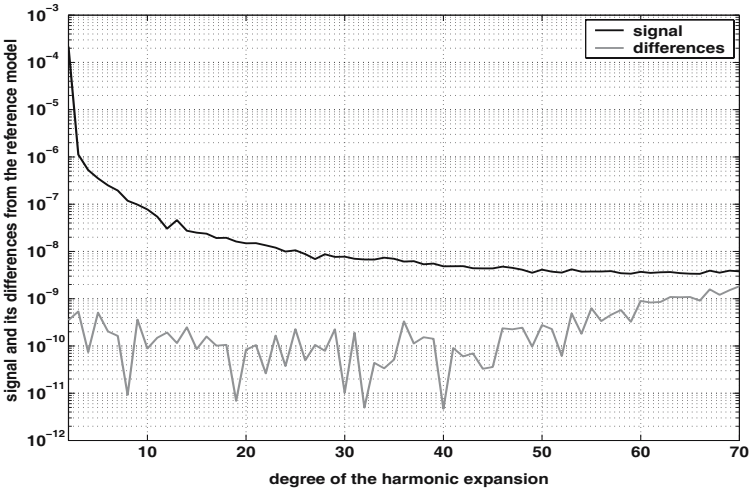

Fig. 8. Recovered coefficients and their difference to the EIGEN-GRACE02S model

5 Conclusions

Global mapping of the Earth's gravity field through the Newtonian equation of motion, see (9), combined with spectral representation, see (23), and integral representation, see (25), respectively, of the geopotential was discussed in this article. This approach represents one option for processing of the SST data of type GRACE as well as those of other satellite missions. In view of other known methods used currently in processing the SST data for geopotential recovery, the proposed approach has some significant advantages, namely simple interpretation of the relationship between observations and the unknown Stokes coefficients of the geopotential without any orbit geometry assumptions, a priori information or boundary surface, see also (Reubelt et al., 2003) and (Austen and Grafarend, 2005) for further details. On the other hand, one has to solve potentially weak points of the approach among which the most important one is handling the observation noise in the HL-SST data used for computation of the inter-satellite velocity. Due to correlated noise in the HL-SST data, the differentiation of the satellites' positions does not seem to represent any real problem to the approach.

Extensive numerical testing of the approach revealed some of its main characteristics, namely stability and sensitivity to various observation errors expected to be a part of real data. Although simulating actual errors in all their complexity is very difficult, some realistic scenarios suggest that the approach could be used for recovery of the geopotential coefficients up to degree and order of 120. Note that the time-varying component of the gravitational field was targeted with expected 30-day batches of data to be processed. From this point of view, the performance of the approach and its computer realization

seems to be quite satisfactory fulfilling initial requirements of the project. Even the modified approach using the gradiometric observation equation is applicable with additional advantages of this method, see Keller and Sharifi (2005) for details.

Finally, the initial processing of the actual GRACE data provided some reasonable results proving the applicability of the proposed method for the analysis of real data. The mean difference between recovered solution and the EIGEN-GRACE2S model of the GFZ Potsdam reached the global value of 27 cm. It should be stressed that these intermediate results were obtained for a relatively small sample of data (30-day data sampled at 30 seconds), very small number of outliers removed and not all the effects included in the model. Taking into the account a large difference in the amount of input data and methodology used in their processing, this result seems to be quite promising for future investigations in this field at the Geodetic Institute of the Stuttgart University.

Acknowledgement. This is publication No. GEOTECH-151 of the programme GEOTECHNOLOGIEN of BMBF and DFG, Grant No. 03F0326A. The financial support is gratefully acknowledged as well as numerous thoughtful comments of KH. Ilk.

References

Abramowitz M, Stegun CA (1972) Legendre functions. Handbook of mathematical functions with formulas, graphs and mathematical tables. Dover, New York.

Ardalan AA, Grafarend EW (2004) High-resolution regional geoid computation without applying Stokes's formula: a case study of the Iranian geoid. *J Geod* 78: 138-156

Austen G, Grafarend EW (2005) Gravitational field recovery from GRACE data of type high-low and low-low SST. *Adv Geosc* (in press).

Blaha G (1992) Refinement of the satellite-to-satellite line-of-sight acceleration model in a residual gravity field. *Manuscr Geod* 17: 321–333

Grafarend EW, Vaníček P (1980) On the weight estimation in leveling. NOAA Technical Report NOS 86, NGS 17.

IAG SC7 (2001) Satellite gravity field missions: Simulation scenarios. [$ftp://geo@atlas.geod.uni-bonn.de/pub/SC7\_SimulationScenarios$].

Keller W, Hess D (1998) Gradiometrie mit GRACE. *Z Verm* 124: 137-144

Keller W, Sharifi MA (2005) Satellite gradiometry using a satellite pair. *J Geod*: 544-557

Kellogg OD (1929) Foundations of potential theory. Springer, Berlin.

Martinec Z (2003) Green's function solution to spherical gradiometric boundary-value problem. *J Geod* 77: 41-49

McCarthy DD, Petit G (2004) IERS Conventions (2003). IERS Technical Note 32. Verlag des Bundesamtes für Kartographie und Geodäsie, Frankfurt am Main.

Reubelt T, Austen G, Grafarend EW (2003) Harmonic analysis of the Earth's gravitational field by means of semi-continuous ephemeris of a Low Earth Orbiting GPS-tracked satellite. Case study: CHAMP, *J Geod* 77: 257-278

Rummel R, Reigber C, Ilk KH (1978) The Use of Satellite-to-Satellite Tracking for Gravity Parameter Recovery, Proceedings of the European Workshop on Space Oceanography, Navigation and Geodynamics, ESA SP-137: 153-161

Rummel R (1980) Geoid heights, geoid height differences, and mean gravity anomalies from low-low satellite-to-satellite tracking – an error analysis. Report No. 306, Department of Geodetic Science and Surveying, Ohio State University, Columbus.

Tapley BD, Reigber C (1998) GRACE: A satellite-to-satellite tracking geopotential mapping mission. Proceedings of the Second Joint Meeting of the International Geoid and Gravity Commisions, Trieste, September 7-12.

van Gelderen M, Rummel R (2001) The solution of the general geodetic boundary value problem by least squares. *J Geod* 75: 1-11